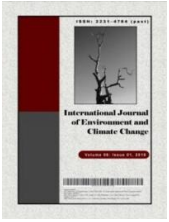

International Journal of Environment and Climate Change

8(2): 96-117, 2018; Article no.IJECC.2018.008
Previously known as British Journal of Environment & Climate Change
ISSN: 2231–4784

Introducing a Modificated Local Model of MODIS with Respect to Radiosonde Data, and Estimation of LWIR Radiation Transmission

Jabar Saydi[1*], Javad Khalilzadeh[1], Safa Khazaei[2] and Mehdi Momeni[3]

[1]Center of Optic and Laser Researches, Faculty of Science, Imam Hossein University, Tehran, Iran.
[2]Faculty of Passive Defense, Imam Hossein University, Tehran, Iran.
[3]Faculty of Technical and Engineering, University of Isfahan, Isfahan, Iran.

Authors' contributions

This work was carried out in collaboration between all authors. Author JS designed the study, performed the data analysis and wrote the first draft of the manuscript. Author JK managed the analyses of the study. Authors SK and MM managed the literature searches. All authors read and approved the final manuscript.

Article Information

DOI: 10.9734/IJECC/2018/v8i227144

Original Research Article

Received 13th January 2018
Accepted 16th March 2018
Published 7th June 2018

ABSTRACT

Aims: Using a latitude dependent local corrected model and based on MODIS data around Mehrabad Synoptic Station of Tehran, the spectral radiance in long wavelength infrared region was modeled and calculated for total upward and downward radiation flux and direct downward radiation flux for cold and hot seasons.
Study Design: Design of the study includes the calculations of local atmospheric profile of the subjected region by radiosonde data, calculations of the atmospheric profile by MODIS data for same region. It presents a latitude dependent relation for modifying the MODIS data of any point which properly could be used instead of radiosonde data at that point and finally model and calculate LWIR's total emitted flux at different heights for the area around subjected region with local profile for both hot (June, July, August) and cold (January, February, March) seasons.
Place and Duration of Study: Department of Optic and Laser, Faculty of science, I. H.U University, between February 2016 and December 2017.
Methodology: The radiosonde and MODIS raw data of 13 stations with different latitudes in 1995-2015 were used for modification purpose. By applying statistic calculations on raw data, the atmospheric profile was extracted. Radiosonde data were not available in any points of a region, while the MODIS data were available. A latitude dependent relation is presented in this work for modifying the MODIS data of any point which properly could be used instead of radiosonde data at that point.

**Corresponding author: E-mail: jabbarsaydi@gmail.com;*

Results: The results were compared and assessed with the default profiles of sub-arctic winter and tropical models. The RMSEs for total upward, downward, and direct radiation fluxes in terms of wavelength in long wavelength infrared in cold and hot seasons were 2.45 $Wm^{-2}\mu^{-1}$ and 1.722 $Wm^{-2}\mu^{-1}$, respectively.

Conclusion: The results showed that local atmospheric profile plays a key role in modifying atmospheric effects on TIR hyperspectral radiance and their accurate understanding improves the quality and quantity of the radiances reaching a sensor and helps better detection of the spectral signature of the study objectives.

Keywords: Radiation transfer; atmospheric compensation; long wavelength infrared; MODIS.

1. INTRODUCTION

The solar energy, which reaches the Earth's upper atmosphere, has been measured using the best-obtained accuracy so far. However, distribution of this energy in the solar system including atmosphere and Earth's surface is still one of the minimum quantitative parameters required for describing the climatic system of a region. The atmospheric radiation measurements in short wavelength infrared (SWIR) region was to study the spectral extent and features of absorption and scattering of solar radiation in clear and cloudy atmosphere theoretically and experimentally reported in different articles [1-5]. However, the atmospheric radiation measurements in the long wavelength infrared (LWIR) region have not been sufficiently reported despite various applications in the area. Thermal infrared (TIR) data, which are obtained in proportion to spectral emissivity and temperature of environmental targets such as rocky cliffs, earth mines, components of specific gases, grasses, etc. provide complementary information. According to Wien's displacement law, the peak of radiation energy of the earth's temperature range (about 273±70 K) is within the spectral range of 8-14 μ, whereas the spectral range of 3-5 μ is obtained from the radiation of hotter objects (more than 600K) such as fire and volcano lava flow [6,7]. TIR data were used in the numerous studies in the fields of several applications including determining soil and mine properties, estimating energy and soil moisture fluxes, detecting fire of forests and volcanoes, determining natural landscape characteristics, etc. [8-12]. IR technology improvement has led to hyperspectral technique in the thermal region in which some images with hundreds of contiguous spectral channels are obtained. The technology has been applied since 1980s in the visible region, NIR, and SWIR; currently, a limited number of hyperspectral imaging systems is in the LWIR region [13-15]. The spectral signature of TIR is affected by atmospheric effects, target temperature and surface properties. TIR models for calculating spectral signature, which include targets and scopes, include suitable assessment tools for hyperspectral imaging [12]. Radiation atmospheric transmission shows many statements in different forms of absorption, scattering, thermal radiation, emitting energies, and so on. In electromagnetic (EM) wave's propagation in atmosphere due to some atmospheric phenomena that mentioned, received radiation on sensors is different from original radiation of target. This difference must be compensated and received spectrum must be corrected. Local atmospheric model is the primer question for this correction. One of the most important applications of atmospheric correction is in the remote sensing. In the thermal region, the reflected atmospheric emission and the statements of the scattered radiance involve in the spectral signature of targets. The scattered radiance caused by atmosphere and solar radiations including the direct and scattering components of solar energy are modeled in the radiative transfer model. Due to the dynamicity of atmosphere, its effect on the radiated spectral radiance requires understanding the atmospheric profile of the subjected region. Radiosonde data are most suitable to modeling the local atmosphere. But these data are not available in any points of a region, while the MODIS data are available. A latitude dependent relation is presented in this work for modifying the MODIS data of any point, which properly could be used instead of radiosonde data at that point. This research modeled and calculated LWIR's total emitted flux at different heights for the area around MSST with the local profile for both hot (June, July, August) and cold (January, February, March) seasons.

2. METHODOLOGY

2.1 Surface Temperature Calculation

The surface temperature of an object with regard to the energy balance is determined in its surface

finite element. To calculate the surface temperature, thermal model based on time-dependent equation of

$$M_s C_{p,s}\left(\frac{dT_s}{dt}\right) = Q_{cond} + Q_{conv} + Q_{solar} + Q_{emiss} \quad (2.1)$$

is used in which T_s is the surface temperature, M_s is the mass, $C_{p,s}$ is the specific heat of the element of an object surface, Q_{cond} is the conductive heat transfer, and Q_{conv} is the convective heat transfer. Q_{solar} is a combination of direct radiation ($q_{solar,\ direct}$) and scattering radiation ($q_{solar,\ diffuse}$) of sunlight both of which are dependent on the azimuth and elevation angles of the sun. Incident radiation on the surface of the object is dependent on absorption processes and scattering of atmosphere. Solar energy absorbed by the surface with absorption coefficient of α and the surface area of A_s , is expressed as:

$$Q_{solar} = \alpha A_s\left(q_{solar,direct} + q_{solar,diffuse}\right) \quad (2.2)$$

2.2 Thermal Flux of Sun

Sunlight direct radiation reaches the object surface after passing through the atmosphere and can be calculated using radiation transfer equations. Total direct sunlight descending on a horizontal surface is as

$$q_{solar,direct} = \int_0^\infty I_{solar,direct}(\lambda) cos\theta_s \, d\lambda \quad (2.3)$$

where, θ_s is the angle of the sun relative to the surface normal axis. Solar radiation passes through the atmosphere before reaching the target and is multiply scattered and can be calculated with a directional integral. Total scattering solar radiation that descends on the object surface is calculated by

$$q_{solar,diffuse} = \int_0^\infty \int I_{solar,diffuse}(\lambda, \omega).\hat{n}\, d\omega\, d\lambda \quad (2.4)$$

where, $\hat{n}$ is the unit vector perpendicular to the object surface and $d\omega$ is the solid angle.

2.3 Atmospheric Transmittance Model

In this study, we calculate the sun radiance and radiation on the path of propagation towards the target using radiation transfer model for the area around Mehrabad Synoptic Station of Tehran (MSST). In this model, the atmosphere is divided into some homogeneous layers. The temperature of each layer is determined using the local profile average of modified MODIS data at different heights for both hot and cold seasons. Stable gases and water vapour concentrations are calculated as a function of height using relative humidity data and radiosonde air pressure. Radiation transfer patterns model the atmosphere as a number of unique layers. Each of these layers shows meteorological conditions including atmospheric compositions of gases, types of particles, and special scattering phase function as default or by the user. Six global default atmospheric profiles are used in radiative transfer models and no partial information is available about them. In this study, local atmospheric profiles from modified MODIS data are used to calculate the upward and downward total heat flux (direct and scattering) and downward direct heat flux at different heights. In other words, a special different model is necessary in any region to apply atmospheric corrections of remote sensing. This is more important in LWIR range of EM radiation.

2.4 Received Spectral Radiance by Sensor

Here, the received spectral radiance is analyzed in LWIR region. Received spectral radiance includes components of direct emission from the object surface, emission reflected from the object surface due to sunlight radiance, emission scattered from the atmosphere without reaching the object surface. Radiance equations received by the sensor at a wavelength of λ_0 (between λ_1 and λ_2) are expressed as

$$I(\lambda_0) = I_{self,emitted}(\lambda_0) + I^r_{solar,direct}(\lambda_0) + I^r_{solar,diffuse}(\lambda_0) + I_{path}(\lambda_0) \quad (2.5)$$

where, $I_{self,emitted}(\lambda_0)$ is the radiance emitted from the object surface. $I^r_{solar,direct}(\lambda_0)$ and $I^r_{solar,diffuse}(\lambda_0)$ are the radiances reflected due to direct and diffusion radiations of the sun from the object surface. $I_{path}(\lambda_0)$ is the scattered radiance of solar radiation in the atmosphere path which is itself a combination of path emission in addition to the scattering resulted from the atmosphere.

2.4.1 Radiance due to self-emission

Radiance of the object intrinsic emission is calculated by

$$I_{self,emitted} = \int_{\lambda_1}^{\lambda_2} \tau_a(\lambda).\varepsilon(\lambda).I_{\lambda b}(T_s)\, d\lambda \quad (2.6)$$

where $\tau_a(\lambda)$ is the spectral throughput of atmosphere, and $\varepsilon(\lambda)$ is the spectral emissivity of the surface. The intensity of blackbody radiation is obtained from Planck's law

$$I_{\lambda b}(T_s) = \frac{2\pi C_1}{\lambda^5\left(e^{C_2/\lambda T_s} - 1\right)};\ C_1 = 0.59552197 \times 10^8 \left[\frac{W.\mu m^4}{m^2.sr}\right],\ C_2 = 14387.69[\mu m.K] \quad (2.7)$$

where, T_s is the absolute temperature of the surface, and C_1 and C_2 are constant values.

2.4.2 Direct radiation radiance of sun

Spectral Radiance reflected by direct sunlight from the object surface that is directed towards the sensor can be calculated with

$$I^r_{solar,direct}(\lambda_0) = \int_{\lambda_1}^{\lambda_2} \tau_a(\lambda).\rho(\lambda).I_{solar,direct}(\lambda)\, d\lambda \quad (2.8)$$

where, $I_{solar,direct}(\lambda)$ is the spectral intensity of direct solar radiation and $\rho(\lambda)$ is the spectral reflectance of the object that is scattered with respect to the vertical descend of the reflective spectrum radiation.

2.4.3 Diffused radiation radiance of sun

Reflected spectral radiance of the diffused sunlight emission that is guided form a hemisphere surface toward the sensor can be calculated from

$$I^r_{solar,diffuse}(\lambda_0) = \int_{\lambda_1}^{\lambda_2}\int_{2\pi} \tau_a(\lambda).\rho(\lambda).I_{solar,diffuse}(\lambda,\omega)\, d\omega\, d\lambda \quad (2.9)$$

where, $I_{solar,diffuse}(\lambda,\omega)$ is the intensity of diffused solar spectrum.

2.4.4 Scattered radiance through the atmospheric passage

Radiance scattered on the passage through the atmosphere contains molecular Rayleigh scattering in clear atmospheric conditions and Mai scattering in the presence of aerosols (water vapor) and fine particles (dust, smoke). In radiative transfer modeling of the atmosphere, scattered radiance in the passage is obtained by adding up the radiance share of layer of the atmosphere. Radiance scattered between the sensor and the earth object is determined by

$$I_{path}(\lambda_0) = \int_0^S \tau_a(S^*,\lambda)J(S^*,\lambda)\ dS^* \quad (2.10)$$

where, S is the line of sight optical path length of the atmosphere from the sensor to the object. J is the total source containing the intrinsic emitted radiation and scattering of solar radiation.

2.5 Modified MODIS Data

Calculating MODIS data error with respect to radiosonde in 13 states of Islamic Republic of Iran a latitude dependent relation is presented which can use local MODIS instead of radiosonde in any region. Based on statistical regression relation, equations for calculating the temperature, height, and water vapor density were derived as:

$$y_j^H = \hat{y}_j^H + k_{1j}^H\varphi + k_{2j}^H \quad (2.11)$$

$$y_j^T = \hat{y}_j^T + k_{1j}^T\varphi + k_{2j}^T \quad (2.12)$$

$$y_j^W = \hat{y}_j^W + k_{1j}^W\varphi + k_{2j}^W \quad (2.13)$$

where *H* is the height, *T* is the temperature. *W* is the water vapor density, and *j* represents the standard pressure levels. y_j and $\hat{y}_j$ are data values at *j*th pressure level from radiosonde and MODIS respectively. k_{1j} and k_{2j} are constants at *j*th pressure level and φ is latitude (in degree). For instance Fig. 1 represents the height-temperature diagram for radiosonde, MODIS and also modified MODIS data for desired latitude of 31.318 degree. As one could see in Fig. 1 there is a good agreement between modified MODIS and radiosonde data.

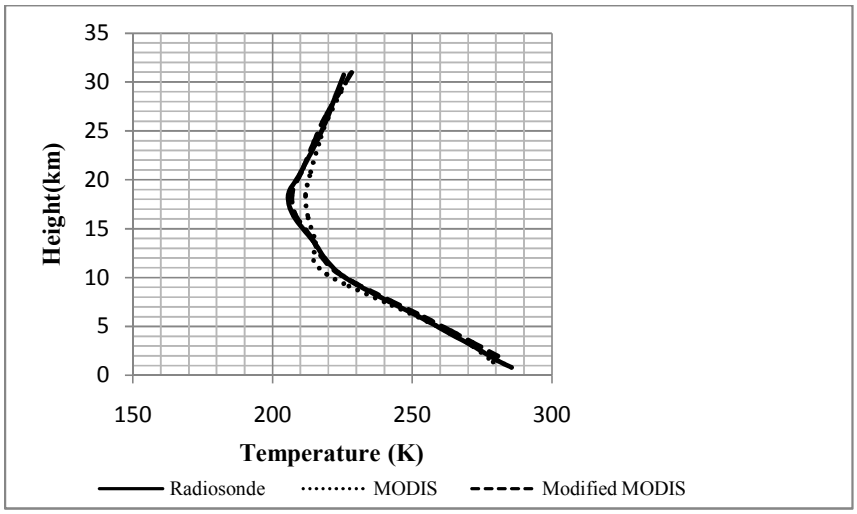

Fig. 1. Height-Temperature diagram for local profile produced by radiosonde, MODIS and modified MODIS data at 31.318° latitude

3. RESULTS AND DISCUSSION

In this study, data profiles of radiosonde are used for two hot and cold seasons to modify atmospheric effects and calculate the resulting radiances. Hence, two general averaged profiles in cold and hot seasons are obtained which can be seen in Fig. 2. As well, these two profiles are compared with six global common profiles. Comparison of local profiles for the subjected region with default profiles of software modeling modification of atmospheric effects in Figs. 2 and 3 shows that there is no good agreement between them. So it is necessary to use local profile data to correct the atmospheric effects on radiation rays and obtain exact spectral radiance. For example comparison of exported profiles in this work with profiles of reference [5]) show that in this reference, profiles are exported only for a few days of June at year 2007. In reference [5]), profiles of height versus temperature calculated until 10-12 kilometers height besides there is a lot of difference between retrieved algorithm and radio sound data but in this research work, calculations and analyses of radio sound data and retrieved MODIS satellite data have investigated until 40 kilometers height for almost two decades and at cold and warm season. Also in this research work, results obtained with the most accordance and least error. In this research, we also modeled and calculated the total flux emitted upward in the LWIR region with local profiles and compared with default profiles so that until now, no similar research have reported.

The radiation emitted from the surface in all directions including direct and scattered radiation (total flux emitted upward) in the LWIR region is shown in Figs. 4 to 11 using local profiles in cold and hot seasons and different heights of the atmosphere. The obtained results are also compared with default profiles of the software modeling modification of atmospheric effects with almost similar trends. Here, local profile in cold and hot seasons is assessed in comparison with default profiles of sub-arctic winter and tropical models. According to Fig. 4, it can be seen that the total upward flux on the ground surface and at an altitude of 10 kilometers have similar trends in hot and cold seasons but as it is expected the total flux emitted upward at an altitude of 10 kilometers is less than the total upward flux on the earth's surface due to the atmospheric weakening the passage of emitted radiation. The amount of upward emitted flux in local profile in cold and hot seasons is higher than default profiles of sub-arctic winter and tropical models. More accurate understanding of atmospheric parameters in different layers in local profile model leads to improvements in atmospheric effects and thus increases the flux of upward emitted radiations. Graphs shown in Fig. 5 demonstrate that the total flux emitted at ground level and a height of 2 km are in good agreement with each other for cold and hot seasons and the curves are perfectly smooth. However, the graphs in Fig. 3 have remarkable differences. Although the graph of the total flux emitted from the Earth's surface is flat, the total flux emitted at an altitude of 10 kilometers has some dipping

due to absorption of atmospheric gases such as ozone in the upper atmosphere. Fig. 6 shows the total flux emitted at altitudes of 1 and 2 kilometres from the ground for cold and hot seasons with local and default profiles. Total emitted radiations in Fig. 6 are in good agreement with each other. But as the total flux is calculated from the earth surface to higher altitudes, the emitted thermal radiation curve becomes rougher. Fig. 7 shows the total emitted flux for altitudes of 2.5 and 3 kilometers from the Earth's surface for cold and hot seasons, with local and default profile models. It can be seen that rugged topography gradually grows above these heights.

LWIR total flux emitted downward are shown in Figs. 8 – 11 using local and default profiles in hot and cold seasons for different heights. Total LWIR radiation emitted downward, including direct and scattered radiation, is shown in Fig. 8 at an altitude of 10 kilometers of the atmosphere and the earth surface for both cold and hot seasons and local and default profiles. It is seen that the amount of total radiation emitted downward in the cold season is less than the hot season. The amount of total radiation emitted downward in the default profiles of sub-arctic winter and tropical models is much more in comparison with local profile of hot and cold seasons. Total radiations emitted downward at an altitude of 2 kilometers of the atmosphere and the Earth's surface are shown in Fig. 9, in both cold and hot seasons for local and default profiles. The more we select the close or near ground layers of the atmosphere (Figs. 10, 11) the curves of total radiation emitted downward will be in good agreement with each other. This increase in the amount of downward total radiation in the default profile vs. local profile at different heights is due to the exact knowledge of atmospheric compounds and profiles in different layers of the local profile. In situations where the atmosphere is known, the effects of absorption, scattering, and hyper-spectral LWIR radiation radiances can be easily modified and tracked, while this state confronts errors in the default profile which lacks detailed information on the atmosphere of the subjected region.

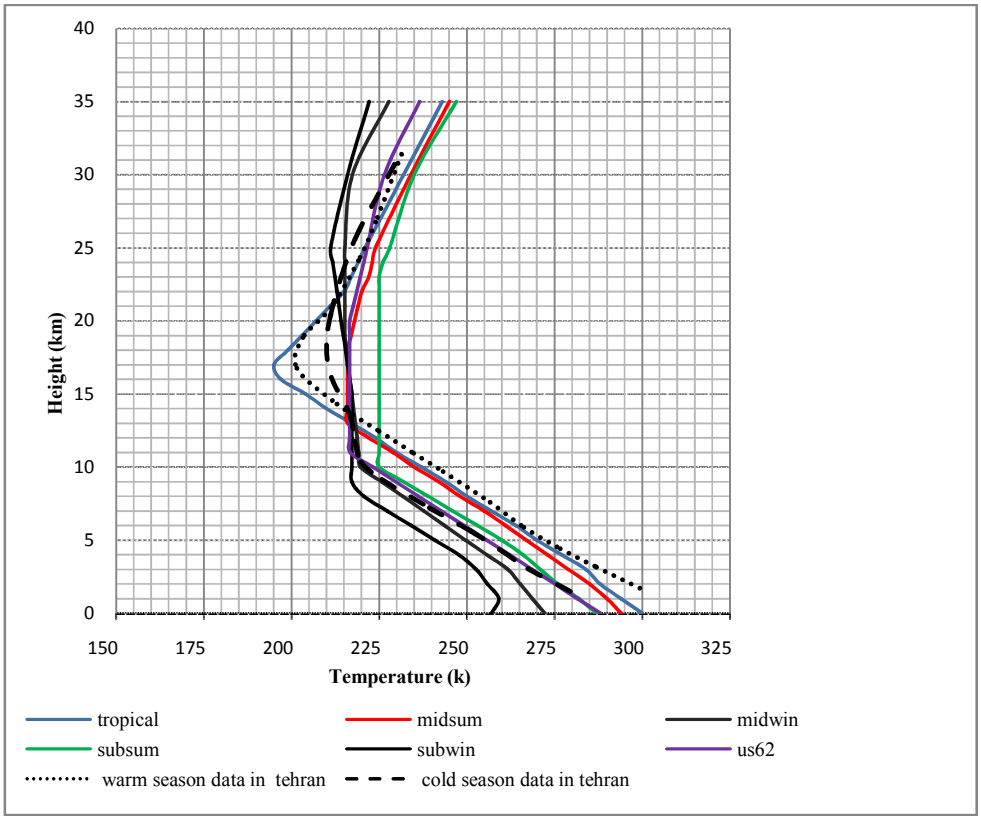

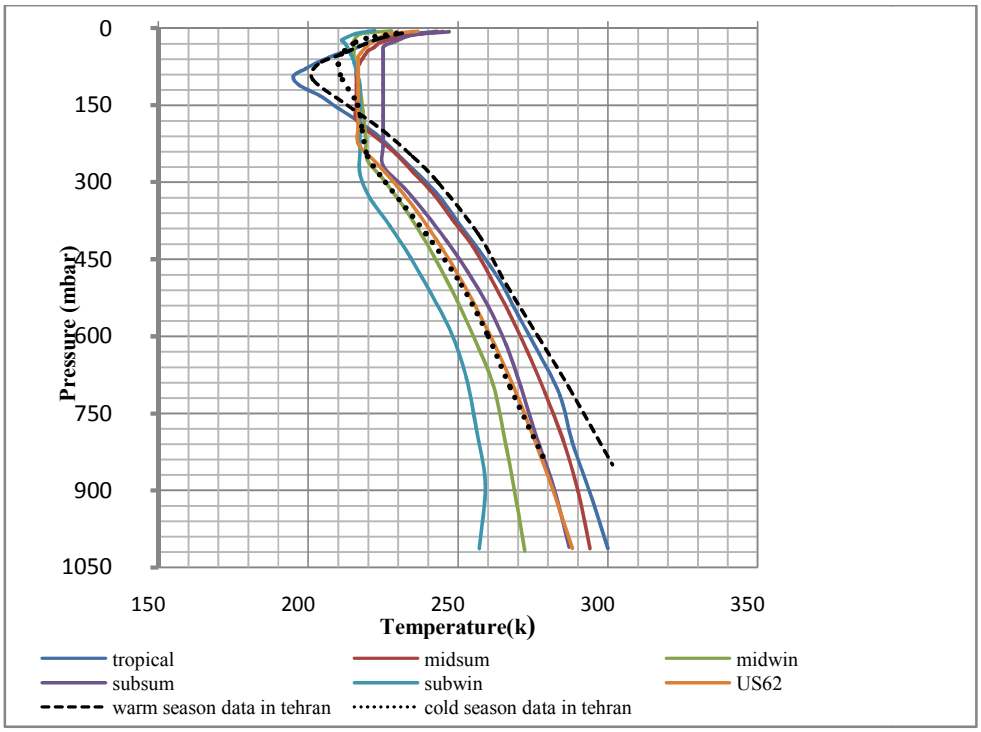

Fig. 2. Height-Temperature (left) and Pressure-Temperature (right) diagrams for local profile in cold and hot seasons, and six global common profiles

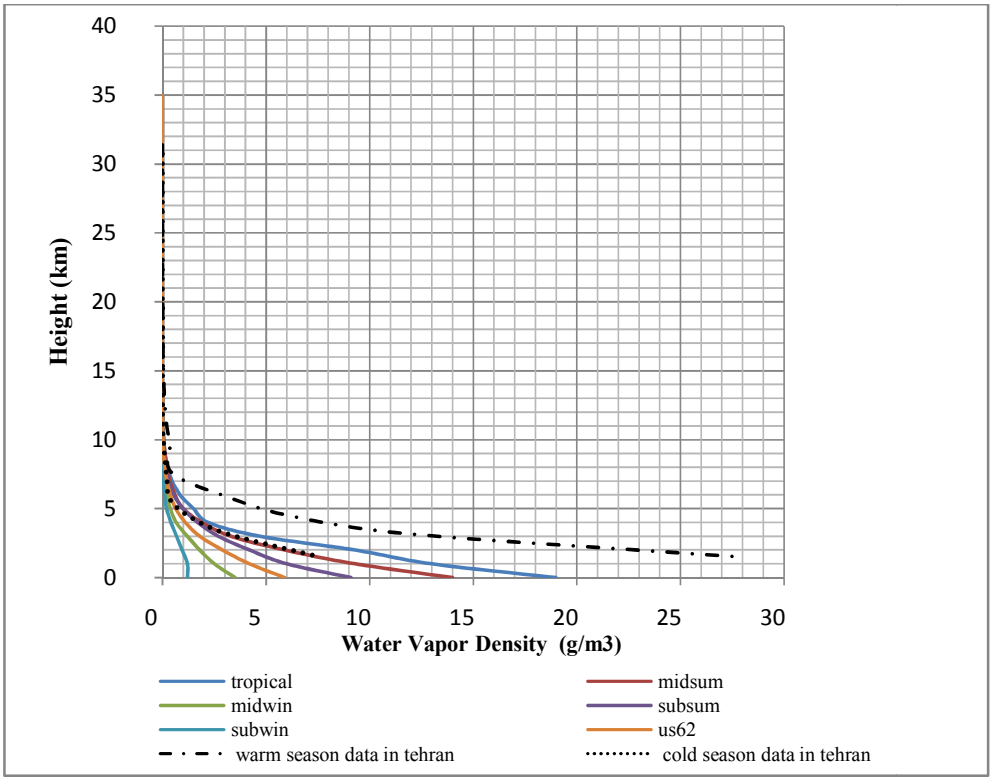

Fig. 3. Height-Water vapor density diagram for local profile in cold and hot seasons and six global common profiles

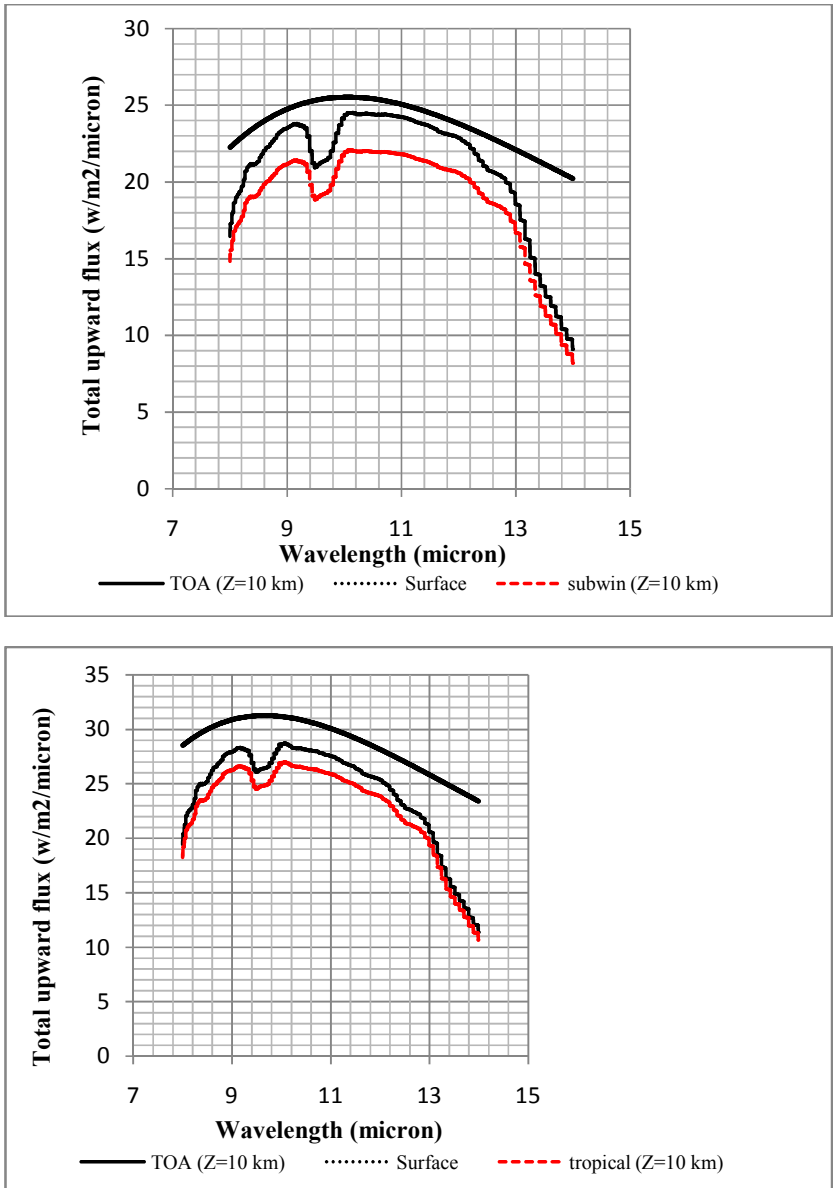

Fig. 4. Total upward flux versus wavelength by cold (left), and hot (right) season profiles in comparison with sub-arctic winter default profile on the ground surface and at altitude of 10 kilometers

Direct downward LWIR radiation flux that is emitted downward from the sun without interacting with molecules is shown in Figs. 12 and 13 using local and default profiles in cold and hot seasons for different heights. As we get closer to the Earth's surface layers, direct downward radiation flux in the LWIR becomes less but is not however negligible. According to the Figs. 12 and 13 direct downward radiation fluxes in default profiles of models sub-arctic winter and tropical have lower value than the local profiles of cold and hot seasons. Reduction in direct downward radiation flux in default profiles is due to the mismatch in local atmospheric profile with the mentioned default profiles.

Root mean square errors for the upward, downward, and direct total radiant flux in terms of wavelength in LWIR region are respectively shown in Fig. 16 in cold and hot seasons. In the cold season, maximum root mean square error

was almost 2.5 $Wm^{-2}\mu^{-1}$ which was obtained for total flux of the upward emitted radiation. Minimum root mean square error in the cold season was obtained for total flux of direct emitted radiation whose amount was less than 0.1 $Wm^{-2}\mu^{-1}$. Maximum root mean square error in the hot season was almost 1.8 $Wm^{-2}\mu^{-1}$ for total flux of the upward emitted radiation. Minimum root mean square error in the hot season was obtained for total flux of the direct emitted radiation whose amount was less than 0.1 $Wm^{-2}\mu^{-1}$.

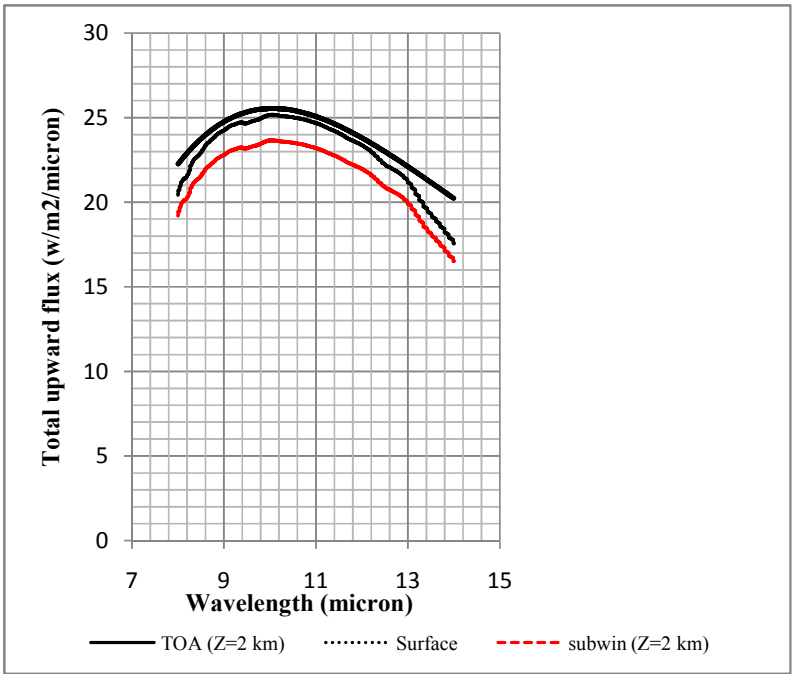

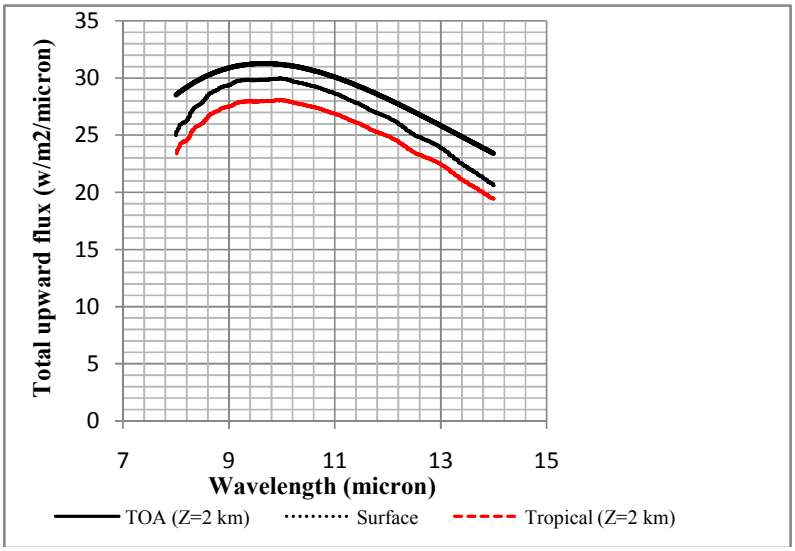

Fig. 5. Total upward flux versus wavelength by cold (left), and hot (right) season profiles in comparison with sub-arctic winter default profile on the ground surface and at the altitude of 2 kilometers

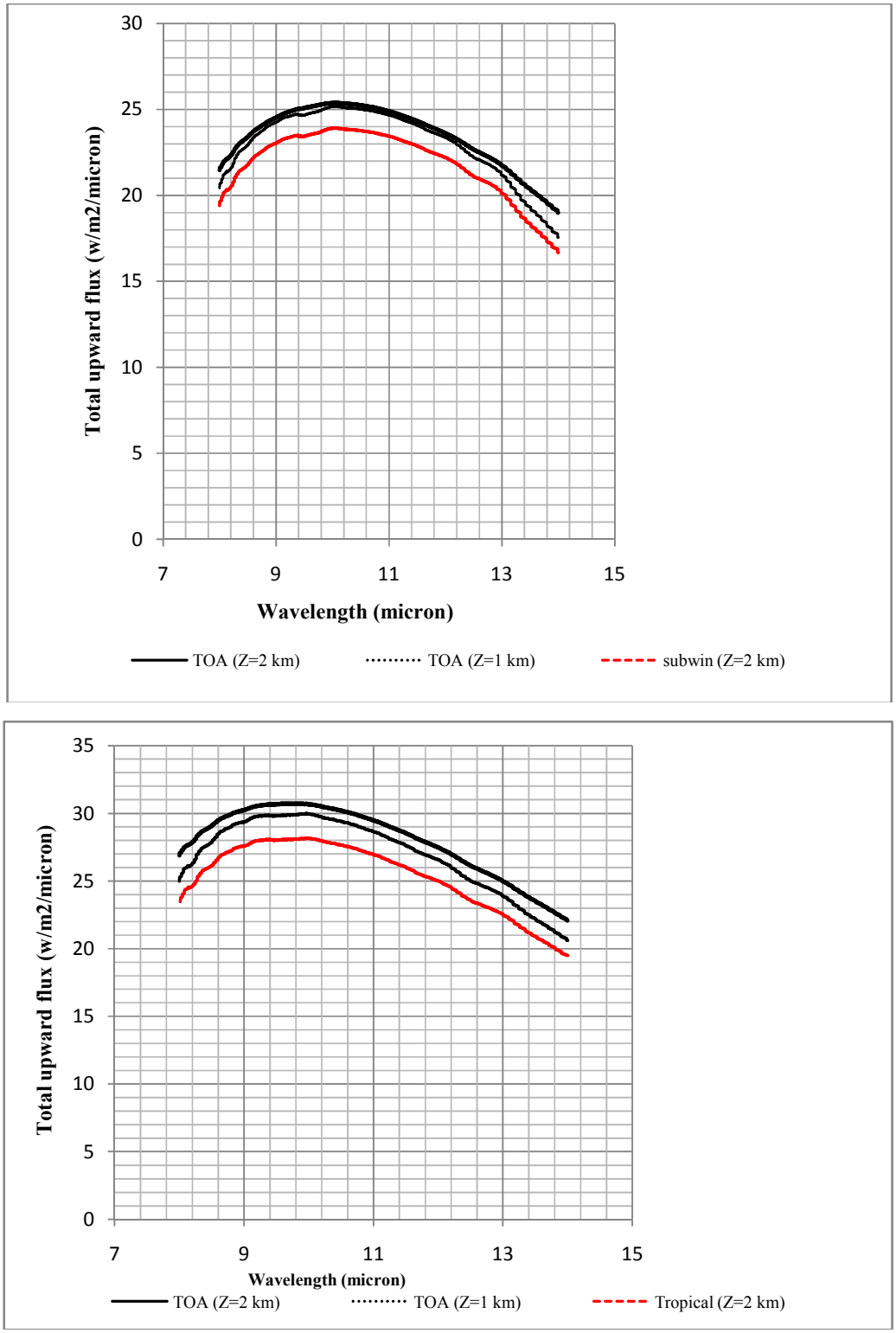

Fig. 6. Total upward flux versus wavelength by cold (left), and hot (right) season profiles in comparison with sub-arctic winter default profile on the ground surface and at altitudes of 1 and 2 kilometers

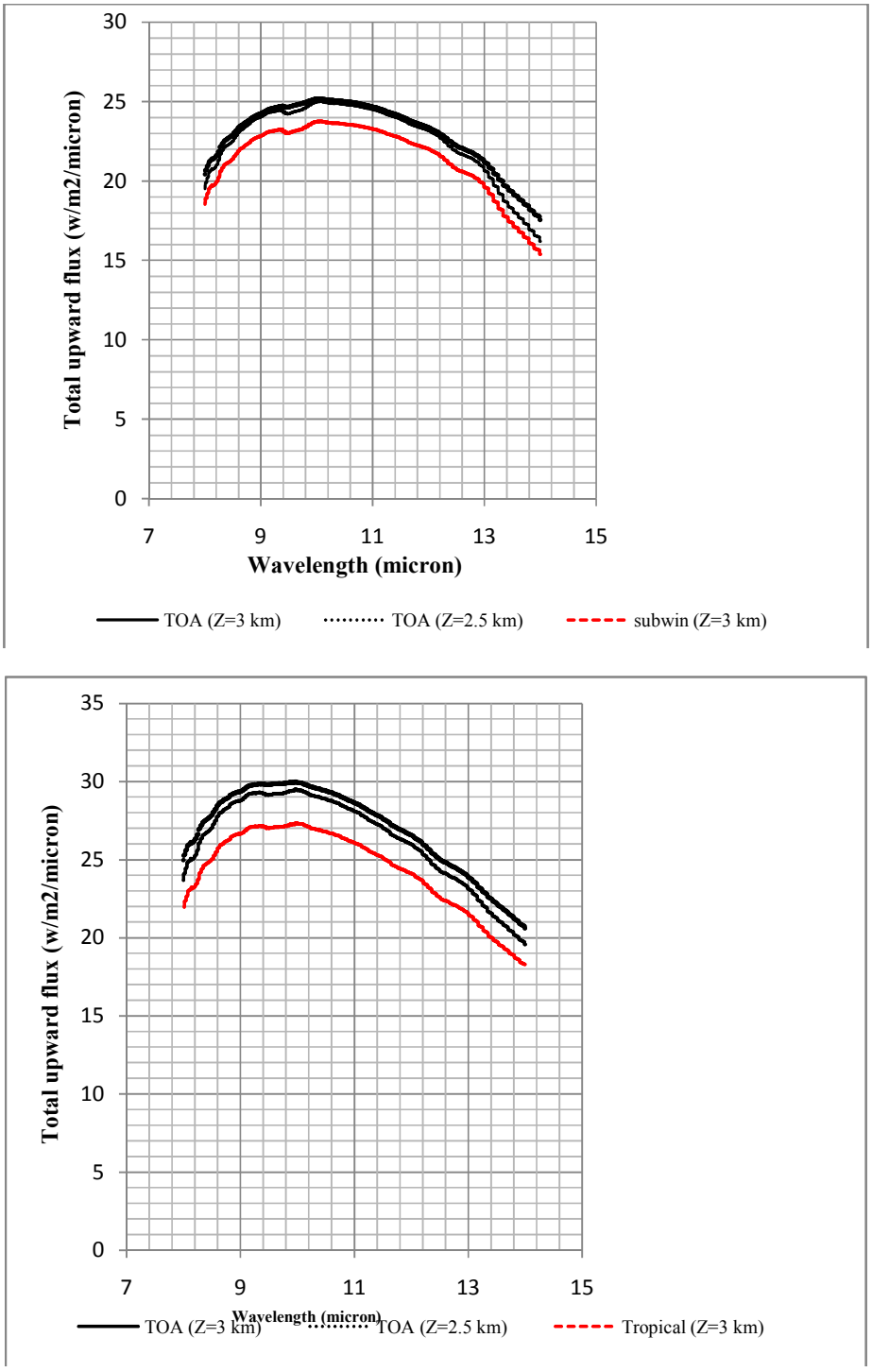

Fig. 7. Total upward flux versus wavelength by cold (left), and hot (right) season profiles in comparison with tropical default profile on the ground surface and at altitudes of 2.5 and 3 kilometers

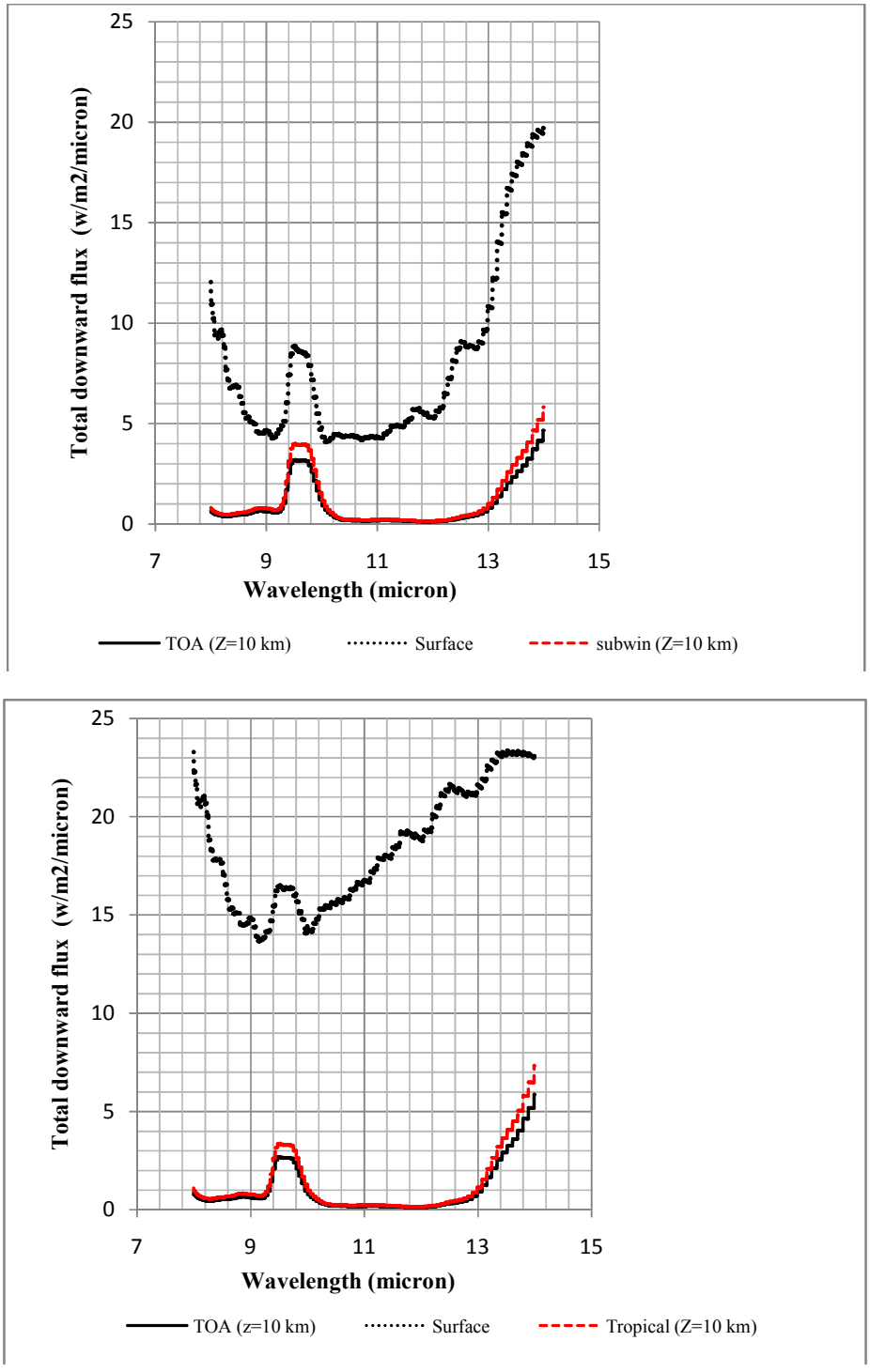

Fig. 8. Total downward flux versus wavelength by cold (left), and hot (right) season profiles in comparison with sub-arctic winter default profile on the ground surface and at altitude of 10 kilometers

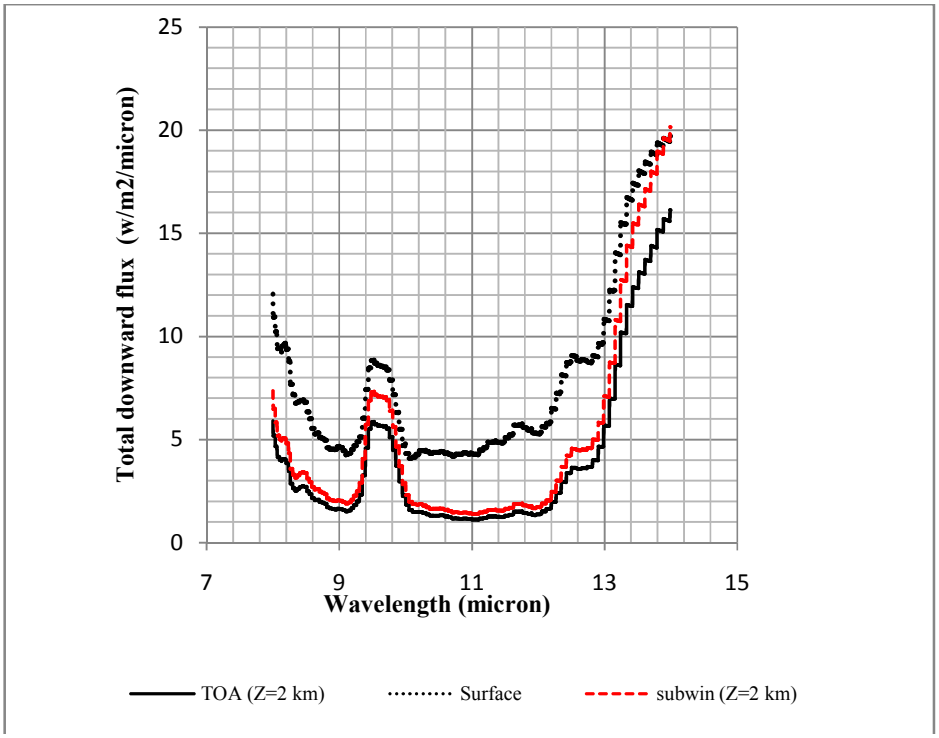

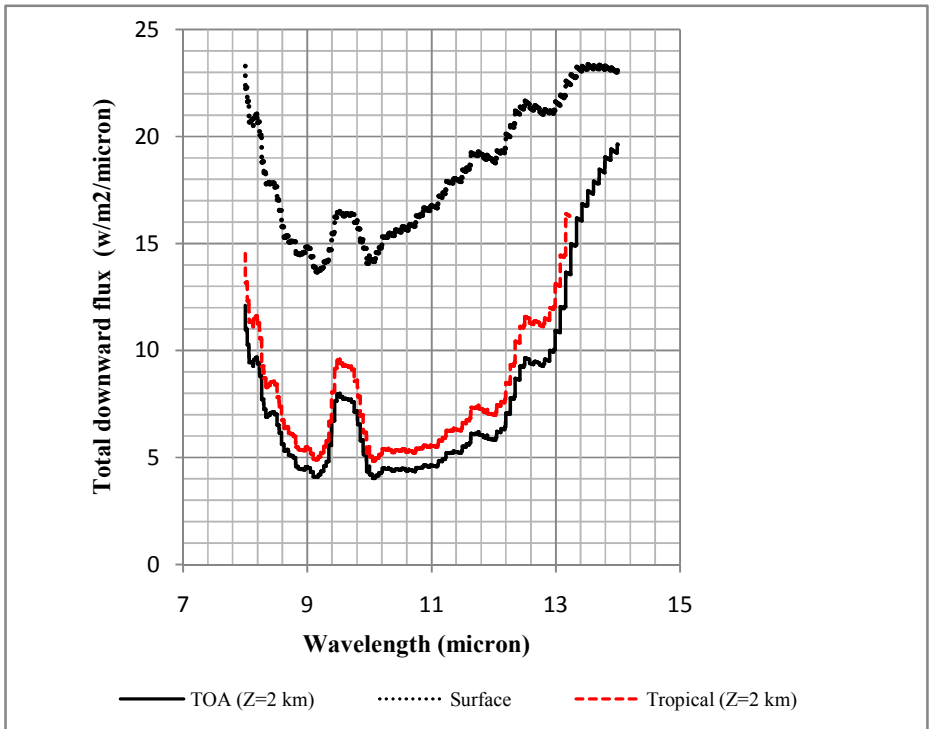

Fig. 9. Total downward flux versus wavelength by cold (left), and hot (right) season profiles in comparison with sub-arctic winter default profile on the ground surface and at altitude of 2 kilometers

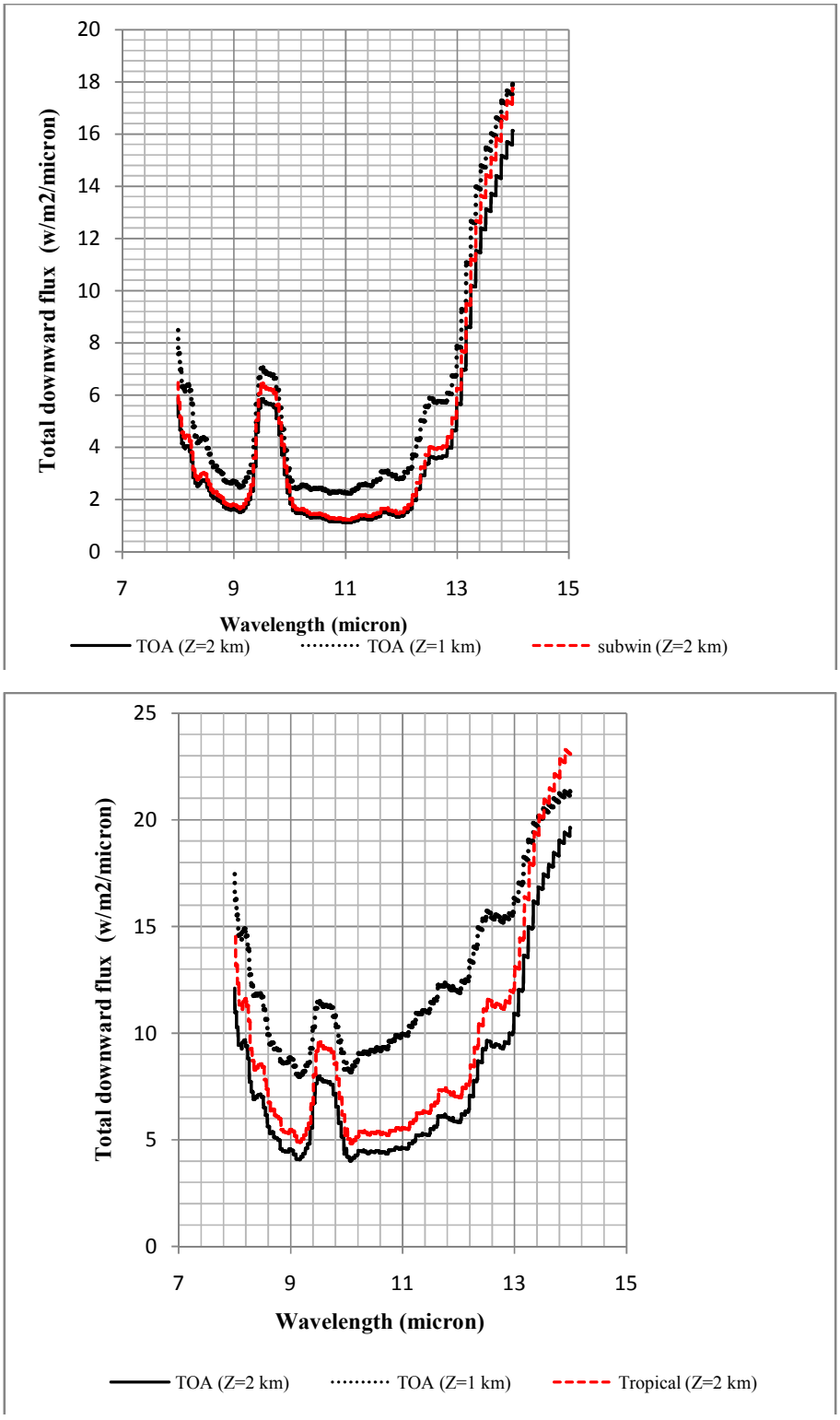

Fig. 10. Total downward flux versus wavelength by cold (left), and hot (right) season profiles in comparison with sub-arctic winter default profile on the ground surface and at altitudes of 1 and 2 kilometers

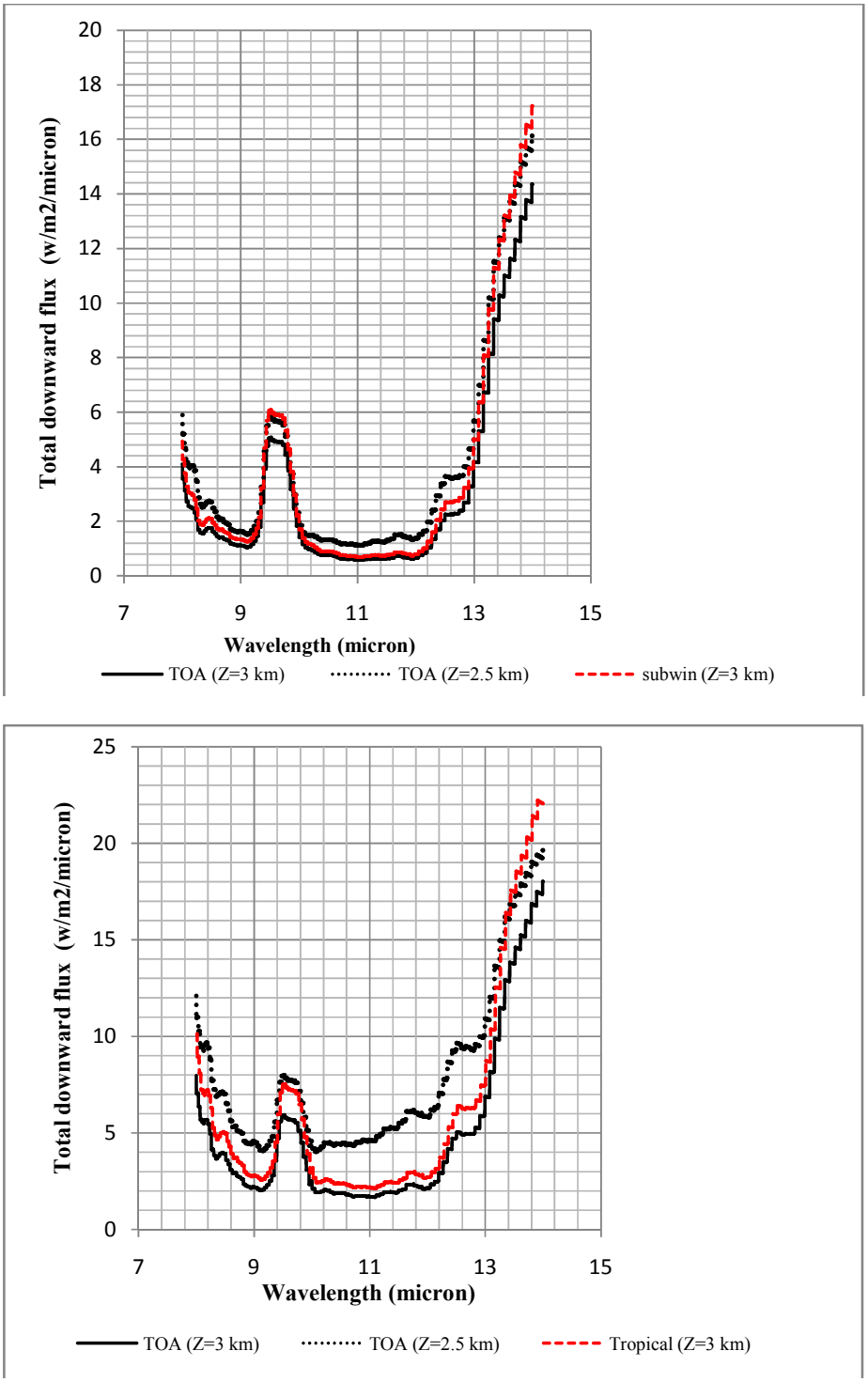

Fig. 11. Total downward flux versus wavelength by cold (left), and hot (right) season profiles in comparison with sub-arctic winter default profile on the ground surface and at altitudes of 2.5 and 3 kilometers

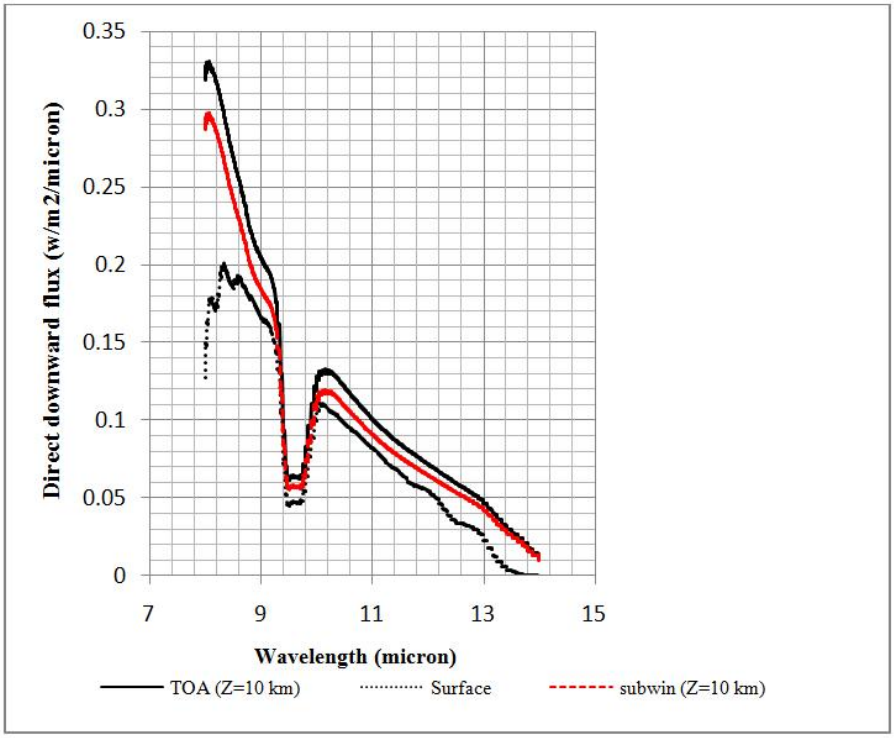

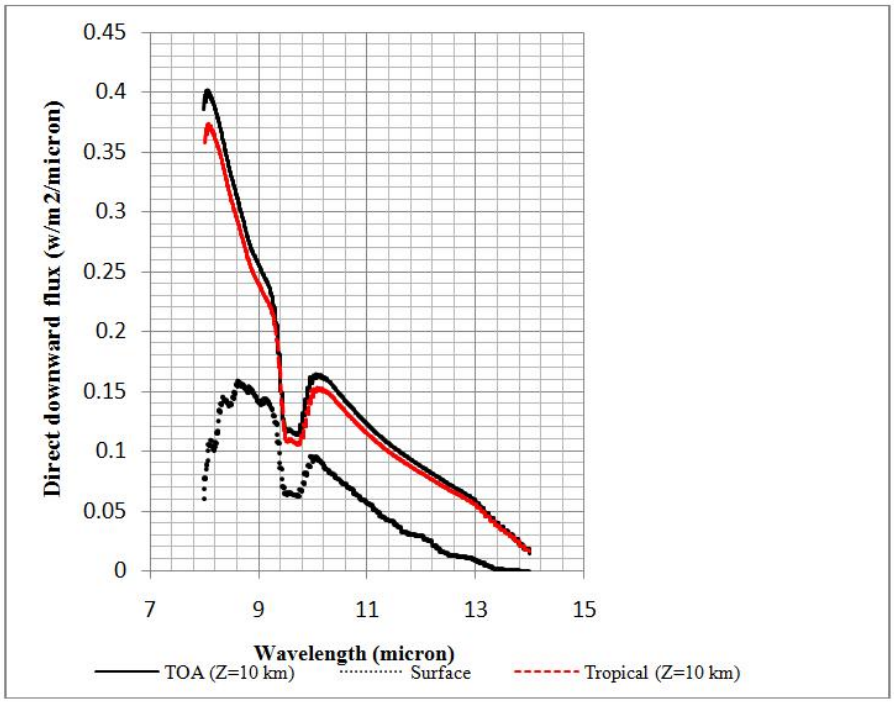

Fig. 12. Direct downward flux versus wavelength by cold (left), and hot (right) season profiles in comparison with sub-arctic winter default profile on the ground surface and at altitude of 10 kilometers

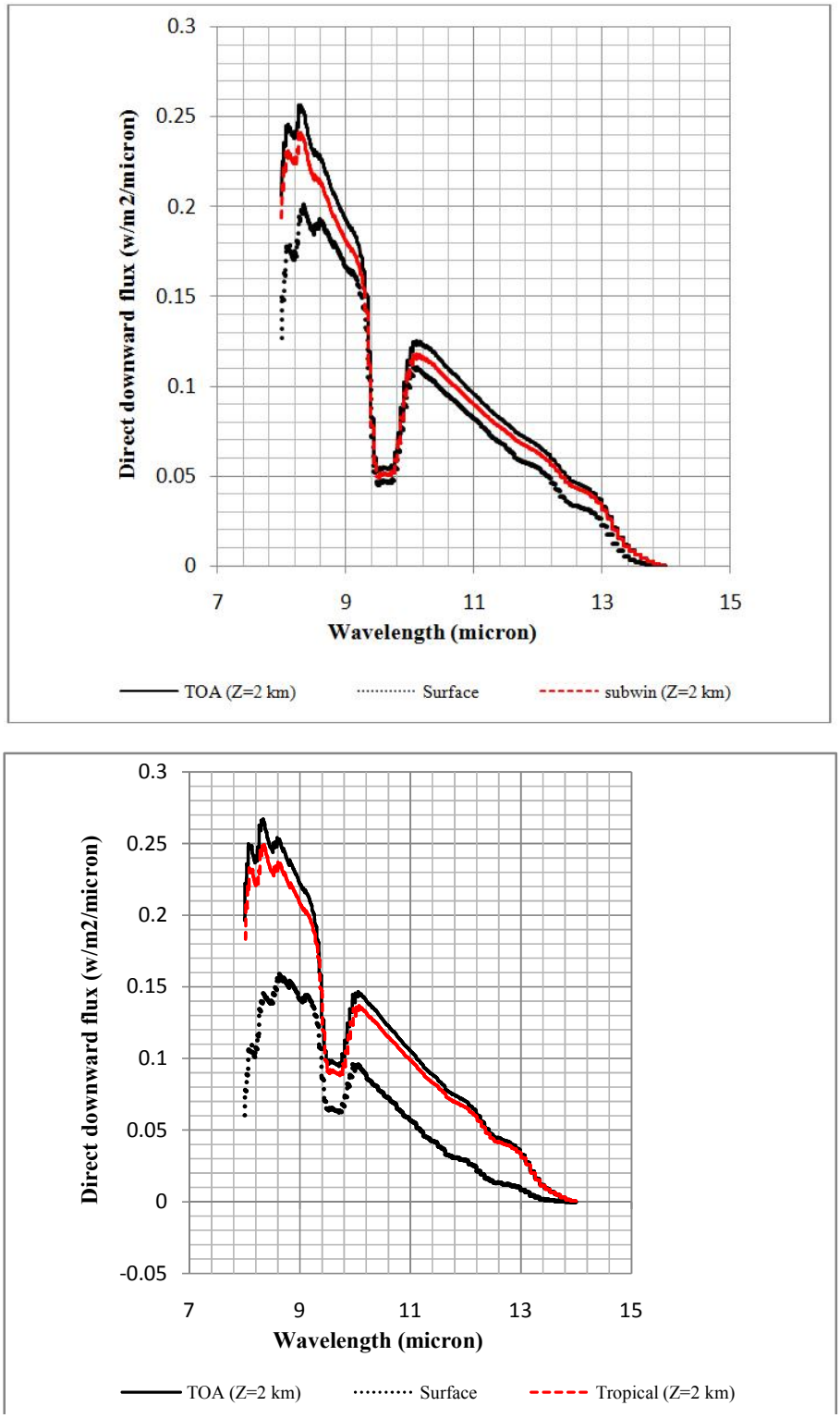

Fig. 13. Direct downward flux versus wavelength by cold (left), and hot (right) season profiles in comparison with sub-arctic winter default profile on the ground surface and at altitude of 2 kilometers

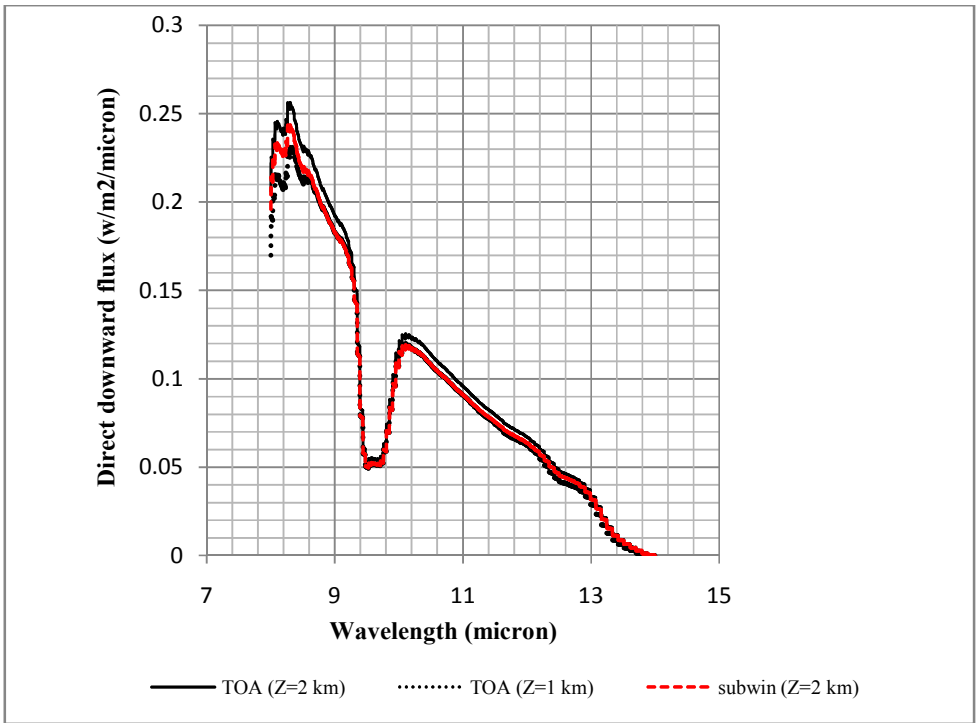

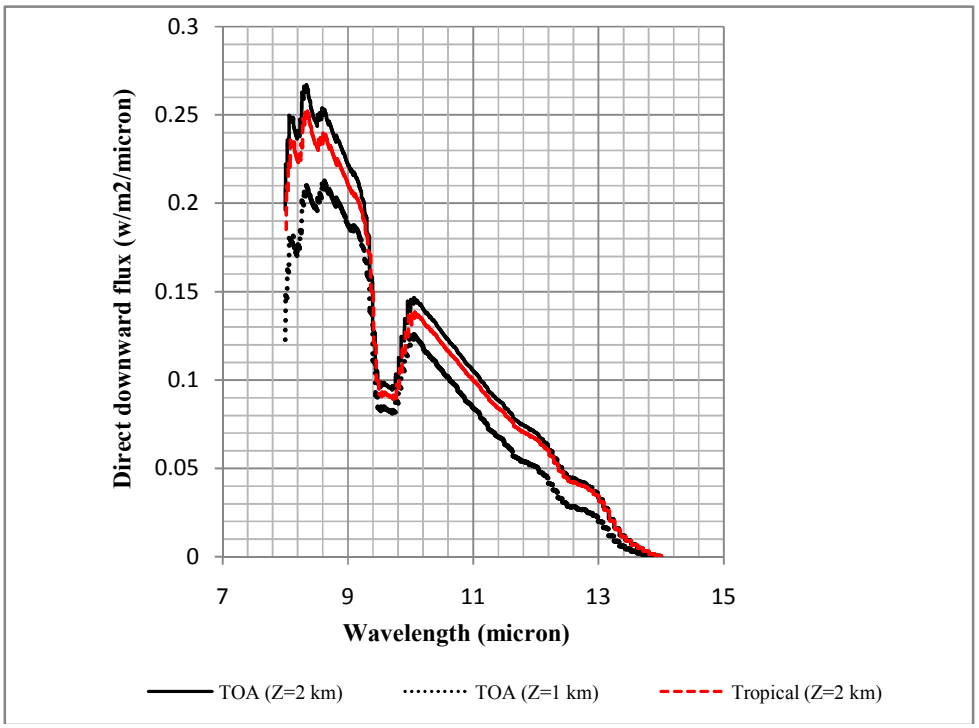

Fig. 14. Direct downward flux versus wavelength by cold (left), and hot (right) season profiles in comparison with sub-arctic winter default profile on the ground surface and at altitudes of 1 and 2 kilometers

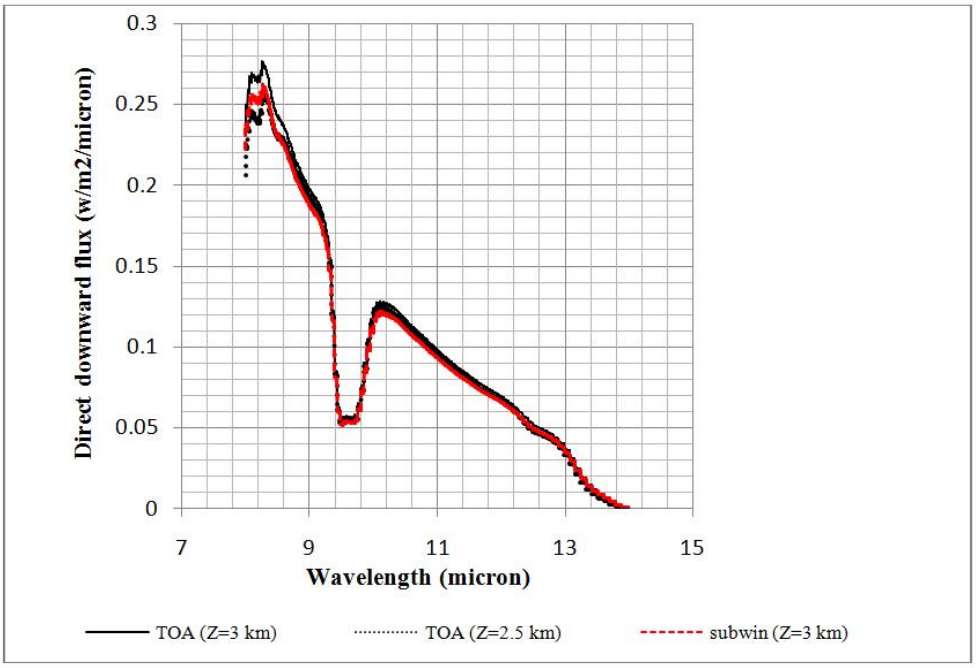

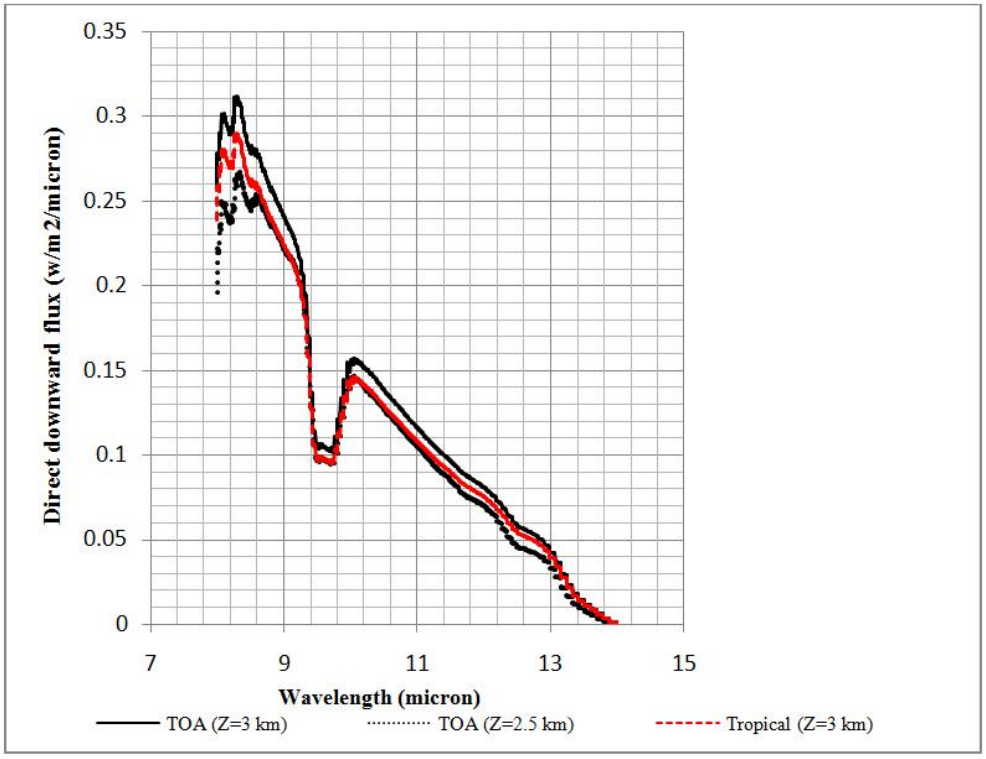

Fig. 15. Direct downward flux versus wavelength by cold (left), and hot (right) season profiles in comparison with sub-arctic winter default profile on the ground surface and at altitudes of 2.5 and 3 kilometers

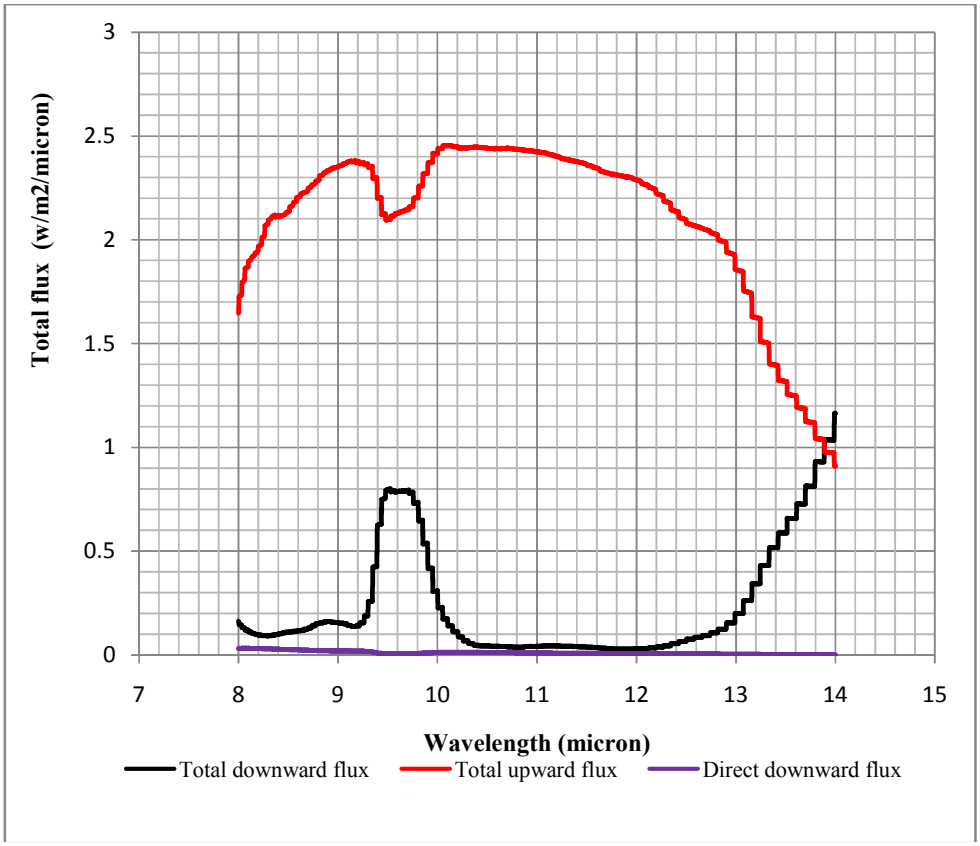

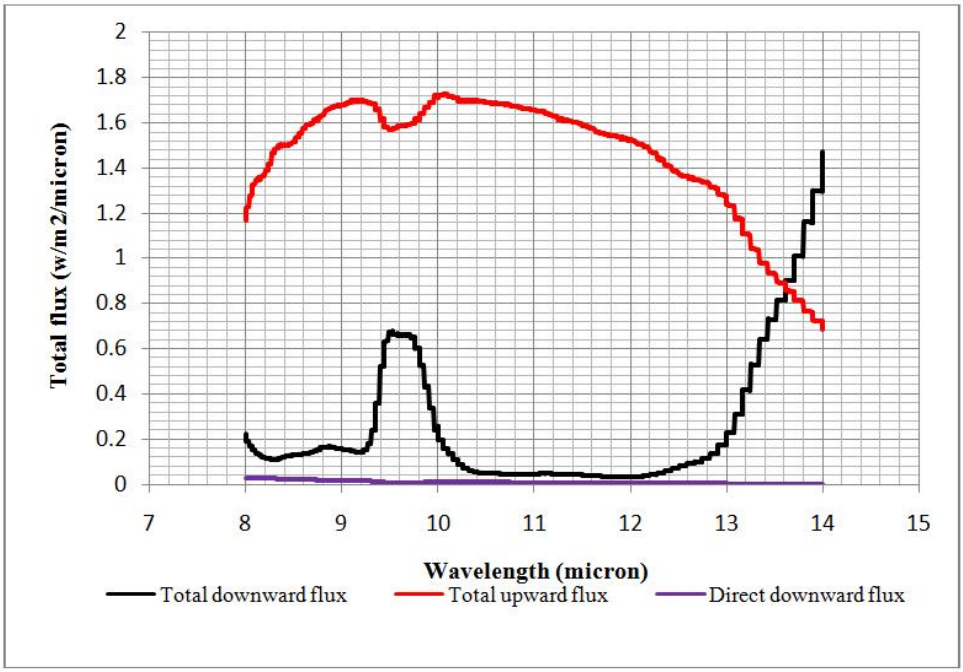

Fig. 16. Root mean square errors for the upward, downward, and direct radiant flux in cold season (left), and hot season (right)

4. CONCLUSION

The MODIS data can be useful anywhere by applying local atmospheric corrections. A latitude dependent local model was developed to modify the MODIS data in the desired region of Iran. The radiosonde data of 13 stations with different latitudes in 1995-2015 were used for modification purpose. Since the radiosonde data are not available for most regions, modified MODIS data could serve as an appropriate local data set for the atmospheric model. We calculated the upward and downward total heat flux (direct and scattering) and downward direct heat flux at different heights using local atmospheric profiles from modified MODIS data and presented herein the results of a comparison of two local and common profiles of atmosphere for compensation of atmospheric effects on thermal infrared spectral image data. The profiles were assessed and compared with the profiles commonly used by researchers as defaults in atmospheric computational codes. The comparison showed that the profile of hot and cold months for the study region, i.e. MSST, was not fully compatible with any of the six global default models. This behaviour indicates that the region's local atmospheric profiles should be used for further accurate results. The results showed that using local profile data would improve the modification of atmospheric effects on hyperspectral radiance in LWIR region. Conditions of the direct downward radiation flux are suitably compatible with local and default atmospheric profiles and the only difference is about some tenth of a Watt per square micron. The difference is due to the better atmospheric modification with local profile; that is, lack of compatibility of local atmospheric profile with the default profiles. The research shows that local atmospheric profile plays a key role in modifying atmospheric effects on TIR hyperspectral radiance and their accurate understanding improves the quality and quantity of the radiances reaching a sensor and helps better detection of the spectral signature of the study objectives. Remote sensing (especially by LWIR waves due to its dependence on inherent radiation of materials) is a nowadays method to data acquisition from different environmental, geographical, mineral, military and so on, targets. Climate change and atmospheric condition have essential effect on such a data acquisition.

COMPETING INTERESTS

Authors have declared that no competing interests exist.

REFERENCES

1. Strawa A, Gore WJY. Atmospheric radiation measurements enhanced shortwave experiment: Experimental and data details. J Geophys Res. 1997;102 D25: 29929-37.
2. Kiehl JT, Tremberth KE. Earth's annual global mean energy budget. Bull Am Meteorol. 1997:78;197-208.
3. Valenzuela A, Olmo FJ, Lyamani H, Anton M, Quirantes A., Alados-Arboledas L. Aerosol radiative forc Figuring during African desert dust events (2005–2010) over Southeastern Spain. Atmosph Chem Phys. 2012;12:10331-51.
4. Bendix J, Thies B, Naußß T, Cermak J. A feasibility study of daytime fog and low stratus detection with TERRA/AQUA-MODIS over land. Meteorol Appl. 2006;13:111–25.
5. Rahimzadegan M, Mobasheri MR, An attempt for improving MODIS atmospheric temperature profiles products in clear sky. Meteorol Appl. 2011;18:181–7.
6. Ogashawara I, Bastos VSB. A quantitative approach for analyzing the relationship between urban heat islands and land cover. Remote Sens 2012;4:3596-3618.
7. Jun-Hyuk Ch, Tae-Kuk K. Study on the spectral transmission characteristics of MWIR through the atmosphere. Image Signal Process Remote Sens. 2007;12:6748.
8. Eisele A, Lau I, Hewson R, Carter D, Wheaton B, Ong C, Cudahy TJ, Chabrillat S, Kaufmann H. Applicability of the thermal infrared spectral region for the prediction of soil properties across semi-arid agricultural landscapes. Remote Sens. 2012;4:3265-86.
9. Frey CM, Parlow E. Flux measurements in Cairo Part 2: On the determination of the spatial radiation and energy balance using ASTER satellite data. Remote Sens. 2012;4:2635-60.
10. Carter A, Ramsey M. Long-term volcanic activity at Shiveluch Volcano: Nine years of ASTER space borne thermal infrared observations. Remote Sens. 2010;2:2571-83.
11. Sobrino JA. Thermal remote sensing from Airborne Hyperspectral Scanner data in the framework of the SPARC and SEN2FLEX projects: An overview. Hydrology Earth Sys Sci. 2009;13:2031-37.

12. Schlerf M, Rock G, Lagueux P, Ronellenfitsch F, Gerhards M, Hoffmann L, Udelhoven T. A hyperspectral thermal infrared imaging instrument for natural resources applications. Remote Sens. 2012;4:3995-4009.
13. Christensen PR, Band field J L, Hamilton VE, Ruff SW, Kieffer HH, Titus TN, Greenfield M. Mars global surveyor thermal emission spectrometer experiment: Investigation description and surface science results, J Geophys Res. 2001;106:23823-71.
14. Lucey PG, Williams TJ, Hinrichs JL, Winter ME, Steutel D, Winter EM. Three years of operation of AHI: The University of Hawaii's airborne hyperspectral imager. Proc SPIE 2001;4369:112-20.
15. Hackwell JA, Warren DW, Bongiovi RP, Hansel SJ, Hayhurst TL, Mabry DJ, Sivjee MG, Skinner JW. LWIR/MWIR imaging hyperspectral sensor for airborne and ground-based remote sensing. Proc SPIE 1996;2819:102-7.

© 2018 Saydi et al.; This is an Open Access article distributed under the terms of the Creative Commons Attribution License (http://creativecommons.org/licenses/by/4.0), which permits unrestricted use, distribution, and reproduction in any medium, provided the original work is properly cited.